Chapter 3
Mathematical Modeling of Flexoelectric Effect

To study the flexoelectric effect, a three-point excitation model for a piezoelectric element with a proof mass at its center was selected. This type of excitation occupies an "intermediate" place between cantilever- and stack-type PEGs. The axial action of the proof mass along the center of the plate leads to an elastic deflection (see Fig. 3.1), which causes compression of the upper and tension of the lower near-electrode layers, as well as the creation (or modification of existing stationary gradients) of counter-directed gradients of deformation.

The possibility of the occurrence of polarization under the action of the strain gradient was first pointed out by Mashkevich and Tolpygo [103, 168]. They obtained a mathematical expression for the relation between the amplitudes of polarization and the gradient of deformation in an acoustic wave for structures of the diamond type. The first step in describing the phenomenon was undertaken by Kogan [84]. Some symmetry aspects of the description within the framework of the scheme, proposed in [84], were discussed in the work of Indenbom, Loginov, and Osipov [79]. In the same work, an attempt was made to microscopically describe the flexoelectric effect for the case of a static strain gradient. The effect was studied experimentally by Zheludev [185]. The experimentally-obtained value of the proportionality coefficient between the polarization and the strain gradient was four orders of magnitude larger than the rough theoretical estimate.

The purpose of this chapter is to simulate the effect of mechanical loading by using a three-point scheme of bending on the possibility of obtaining an electrical response from unpolarized ferroelectric ceramics plates.

© Springer International Publishing AG, part of Springer Nature 2018

S. N. Shevtsov et al., *Piezoelectric Actuators and Generators for Energy Harvesting*,
Innovation and Discovery in Russian Science and Engineering,
https://doi.org/10.1007/978-3-319-75629-5_3

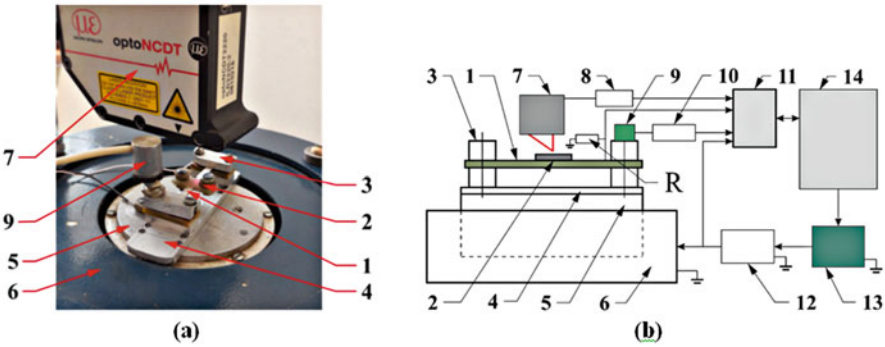

Fig. 3.1 (**a**) General view of the measuring set-up, where 1 is the piezoelectric plate, 2 is the proof mass, 3 is the first fixing point, 4 is the piezogenerator base, 5 is the vibrator working table, 6 is the electromagnetic vibrator, 7 is the optical sensor of linear displacement, and (**b**) its structural scheme, where 1 is the sample under study, 2 is the proof mass, 3 is the first fixing point, 4 is the mounting base, 5 is the shaker's moving table, 6 is an electromagnetic shaker VEBRobotron 11,077, 7 is the optical linear sensor, 8 is the optical sensor controller, 9 is the acceleration sensor ADX 103 (second fixing point), 10 is the acceleration sensor matching device, 11 is the external module of ADC/DAC E14-440D, 12 is the power amplifier, 13 is the functional signal generator, 14 is the computer, *R* is the load resistance

3.1 Investigation of Output Voltage in Unpolarized Ceramics

3.1.1 Samples for Study and Experimental Procedure

Four batches of plates, made from ceramics PZT-19 with the size of $50 \times 4 \times 0.7$ mm^3, were used in this study. The electrodes from the silver were applied to the large surfaces. Before applying the electrodes, samples in batches 2, 3, and 4 were additionally damaged during processing one of the sides using grinding powders with grain sizes of 5, 10, and 20 μm, respectively. Using this method, a different depth of diffusion of Ag was obtained. After the Ag was burned into the surface, metal-ceramic layers with various thicknesses were created on opposite sides. At the boundaries of these layers in batches 2, 3 and 4, gradients of mechanical deformations, as well as tangential compressive stresses, were non-equivalent to the samples in batch 1. Compressive stresses are due to the difference in the temperature coefficients of linear expansion for Ag and ferroelectric ceramics on cooling from 730 °C after burning [158].

Figure 3.1 presents a photograph of the measuring set-up and its structural diagram

The measuring set-up used in this experiment is almost identical to the set-up described in the previous chapter, which was used to determine the output characteristics of the cantilever-type PEG. The main difference is in the device for holding the sample, which provided a cantilever clamp on both sides.

3.1.2 *Results of the Experiment and Discussion*

Figure 3.2 shows the dependence of the electrical response of the plates on the acceleration of the shaker in the presence of the proof mass $M = 3.1$g. The analysis of Fig. 3.2a (for plate # 3 of batch 1 – 3B1) shows that in batch 1 after Ag burning, the gradients of static deformation at the boundaries of cermet layers with a ceramic volume, as well as the tangential compressive stresses in the near-electrode layers create the electric polarization. This polarization is stable to multiple mechanical influences. This conclusion is illustrated by the curves in Fig. 3.2a, the first of which (down) was obtained before, and the second (up) after turning the plate under M on 180°. The output electrical signal from the action of M is due to the compression of the near-surface layer and the tension of the lower layer. In this batch, for each position of the plate surfaces with respect to M, the values of the output voltage were the same. This fact indicates the identity of the created polarizations for opposite faces.

Figure 3.2b demonstrates a 25% increase in the electrical response of the 6B3 sample, when the more defective face is located on the opposite side of M (down). In this case, as in batch 1, the deflection of the plate under M creates a tensile mechanical stress opposite to the existing one, which arises during the formation of the cermet layer at this surface. The difference in the magnitude of the output voltage can be provided by a higher value of polarization at this surface.

The main result of this experiment is that the described polarization originates on opposite surfaces of ceramic plates from PZT-19 when Ag is fired. The values of this polarization depend on the degree of surface roughness before the application of the electrodes. Because the effect is investigated at room temperature in the ferroelectric phase for the PZT-19, it is impossible to unambiguously interpret it as flexoelectrical

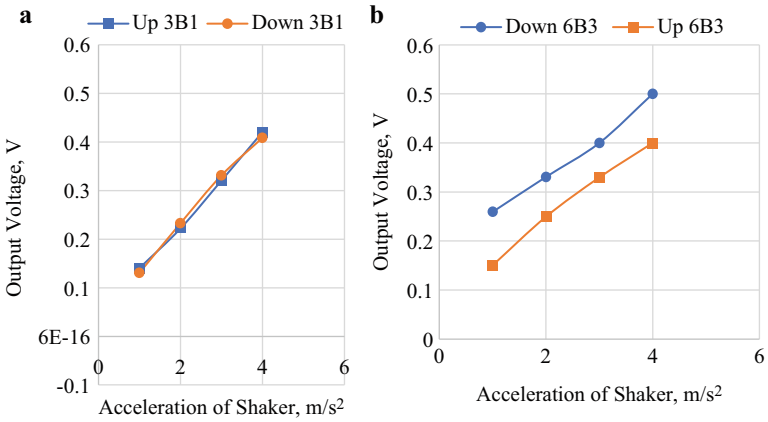

Fig. 3.2 Relationship between electrical response to mechanical impact of $M = 3.1$ g and acceleration of the worktable: before (up) and after (down) rotation of the specimens on 180° in the clamping device: beams from batches #1 (**a**) and #3 (**b**)

and "giant." At the same time, with a high probability, it can arise in a very thin transition layer on the boundary of the cermet layer with a homogeneous array of ceramics. However, its output voltage of 0.5 V for a plate thickness of 0.7 mm without preliminary polarization in an electric field is already of practical interest for creating a multi-layer transducer with thinner plates.

3.2 Investigation of the Flexoelectric Effect in Unpolarized Ceramics

3.2.1 Formulation of the Problem for Flexoelectrical Beam

Most of the works devoted to modeling the flexoelectric effect in solids [1, 76, 100, 102] use the variational approach proposed by Mindlin [110]. We write down the variational principle for an electroelastic body as follows:

$$\begin{aligned}\delta \int_{t_1}^{t_2} dt \iiint_V \left[\frac{1}{2}\rho|\ddot{\mathbf{u}}|^2 - \left(W^L - \frac{1}{2}\varepsilon_0|\nabla\varphi|^2 + \mathbf{P}\cdot\nabla\varphi\right)\right] dV + \\ \int_{t_1}^{t_2} dt \iiint_V \left(\mathbf{q}\cdot\delta\mathbf{u} + \mathbf{E}^0\cdot\delta\mathbf{P}\right) dV + \int_{t_1}^{t_2} dt \iint_S (\mathbf{t}\delta\mathbf{u}) = 0,\end{aligned} \tag{3.1}$$

where V is the volume of the body, ρ is the density, $\mathbf{u}$ is the displacement vector, W^L is the internal energy density, ε_0 is the electric constant, $\mathbf{P}$ is the polarization vector, ϕ is the electric potential, $\mathbf{q}$ is the mass forces, $\mathbf{E}^0$ is the external electric field, S is the surface in which the volume V is enclosed, $\mathbf{t}$ is the surface forces.

In order to account for the influence of the strain gradient, we will use the potential energy density in the form [148]:

$$\begin{aligned}W^L(\mathbf{P}, \boldsymbol{\varepsilon}, \nabla\nabla\mathbf{u}) = \ & \frac{1}{2}\mathbf{P}\cdot\mathbf{a}\cdot\mathbf{P} + \frac{1}{2}\boldsymbol{\varepsilon} : \mathbf{c} : \boldsymbol{\varepsilon} + \mathbf{P}\cdot\mathbf{d} : \mathbf{S} \\ & + \mathbf{P}\cdot\mathbf{f} : \nabla\nabla\mathbf{u} + \frac{1}{2}\nabla\nabla\mathbf{u} : \mathbf{g} : \nabla\nabla\mathbf{u}.\end{aligned} \tag{3.2}$$

where $\mathbf{a}$ is the inverse dielectric susceptibility, $\boldsymbol{\varepsilon}$ is the small deformation tensor, $\mathbf{c}$ is the tensor of elastic moduli, $\mathbf{d}$ is the tensor of piezomodules, $\mathbf{f}$ is the tensor of flexoelectric moduli, $\mathbf{g}$ is a tensor that describes pure nonlocal elastic effects, $\nabla\nabla\,\mathbf{u}$ is the gradient of deformation.

We substitute the expression for the potential energy Eq. (3.2) into the first term of the variational principle in Eq. (3.1):

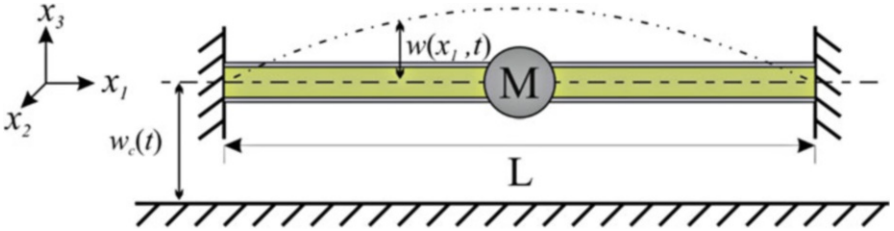

Fig. 3.3 Kinematic scheme of loading of flexoelectric beam

$$\delta \int_{t_1}^{t_2} dt \iiint_V \left[W^L - \frac{1}{2}\varepsilon_0 |\nabla\varphi|^2 + \mathbf{P}\cdot\nabla\varphi \right] dV = \int_{t_1}^{t_2} dt \iiint_V \left(\frac{\partial W^L}{\partial \mathbf{P}}\delta\mathbf{P} + \frac{\partial W^L}{\partial \boldsymbol{\varepsilon}}\delta\boldsymbol{\varepsilon} + \frac{\partial W^L}{\partial(\nabla\nabla\mathbf{u})}\delta(\nabla\nabla\mathbf{u}) \right) dV - \int_{t_1}^{t_2} dt \iiint_V (\varepsilon_0 \nabla\varphi\delta(\nabla\varphi) - \mathbf{P}\delta(\nabla\varphi) - \nabla\varphi\delta\mathbf{P}) dV. \tag{3.3}$$

Since the deformations in this problem are small, to simplify the solution we move from the general formulation of the problem to the one-dimensional case by adopting the Euler-Bernoulli hypotheses.

The excitation of the vibrations of the beam, presented in Fig. 3.3, occurs through the displacement of two clamps relative to a certain plane. Therefore, the absolute displacement of the beam along the coordinate x_3 will consist of the movement of $w_c(t)$ and the relative displacement of the beam $w(x_1, t)$. Taking into account the foregoing, the displacement vector $\mathbf{u}$ takes the following form:

$$\mathbf{u} = \left\{ -x_3 \frac{\partial w(x_1,t)}{\partial x_1}, 0, w(x_1,t) + w_c(t) \right\}^{\mathrm{T}} \tag{3.4}$$

Taking into account the introduced hypotheses, the non-zero components of the strain gradient are $\varepsilon_{11,\,1}$ and $\varepsilon_{11,\,3}$. Since the beam under consideration is sufficiently thin, we neglect $\varepsilon_{11,\,1}$. The deformation gradient $\varepsilon_{11,\,3}$ will cause the separation of centers of positive and negative charges in the unit cell of the material, thereby creating a polarization [53].

Expressions for the components of the strain tensor and the strain gradient, taking into account the introduced hypotheses, take the following form:

$$\begin{aligned}\varepsilon_{11} &= -x_3 \frac{\partial^2 w}{\partial x_1^2}, \\ \varepsilon_{11,3} &= -\frac{\partial^2 w}{\partial x_1^2}.\end{aligned} \tag{3.5}$$

We also take the following simplifications for the polarization vector:

$$\mathbf{P}(x_1, x_3, t) = \{0, 0, P(x_1, x_3, t)\}. \tag{3.6}$$

Taking into account the introduced simplifications and hypotheses for the convenience of writing further calculations, we take the following notation [53]:

$$a = a_{33},\ c = c_{1111},\ d = d_{311},\ f = f_{3113},\ g = g_{113113} \tag{3.7}$$

The density of potential energy takes the following form:

$$W^L = \frac{1}{2} aP^2 + \frac{1}{2} cx_3^2 \left(\frac{\partial^2 w}{\partial x_1^2}\right)^2 - dx_3 P \frac{\partial^2 w}{\partial x_1^2} - fP \frac{\partial^2 w}{\partial x_1^2} + \frac{1}{2} g \left(\frac{\partial^2 w}{\partial x_1^2}\right)^2. \tag{3.8}$$

Suppose that external forces and electric fields are absent. Substituting the expression for the potential energy density Eq. (3.8) into Eq. (3.3), we get:

$$\begin{aligned}&\int_{t_1}^{t_2} dt \iiint_V \rho(\ddot{w} - \ddot{w}_c)\delta w dV + \int_{t_1}^{t_2} dt \iiint_V \left[\left(aP - dx_3 \frac{\partial^2 w}{\partial x_1^2} - f \frac{\partial^2 w}{\partial x_1^2} + \frac{\partial \varphi}{\partial x_3}\right)\delta P + \right. \\ &+ \left(cx_3^2 \frac{\partial^2 w}{\partial x_1^2} - dx_3 P - fP + g \frac{\partial^2 w}{\partial x_1^2}\right)\delta\left(\frac{\partial^2 w}{\partial x_1^2}\right) + \\ &\left. + \left(P - \varepsilon_0 \frac{\partial \varphi}{\partial x_3}\right)\delta\left(\frac{\partial \varphi}{\partial x_3}\right) + \left(-\varepsilon_0 \frac{\partial \varphi}{\partial x_1}\right)\delta\left(\frac{\partial \varphi}{\partial x_1}\right)\right] dV = 0.\end{aligned} \tag{3.9}$$

Since the variation of the polarization δP is arbitrary, then:

$$P = \frac{1}{a}\left(-dx_3 \frac{\partial^2 w}{\partial x_1^2} - f \frac{\partial^2 w}{\partial x_1^2} + \frac{\partial \varphi}{\partial x_3}\right) \tag{3.10}$$

After substitution of Eq. (3.10) into Eq. (3.9) and integrating over the cross-sectional area S, we get:

$$\int_{t_1}^{t_2} dt \int_0^L \rho \mathbf{I_1} \left(\ddot{w} - \ddot{w}_c\right) \delta w dx_1 + \int_{t_1}^{t_2} dt \int_0^L \left\{ \left[\left(c - \frac{d^2}{a} \right) \mathbf{I_3} - \frac{2df}{a} \mathbf{I_2} - \left(\frac{f^2}{a} - g \right) \mathbf{I_1} \right] \frac{\partial^2 w}{\partial x_1^2} + \iint_S \left(\frac{d}{a} x_3 + \frac{f}{a} \right) \frac{\partial \varphi}{\partial x_3} ds \right\} \delta \left(\frac{\partial^2 w}{\partial x_1^2} \right) dx_1 = 0, \tag{3.11}$$

where:

$$\mathbf{I_1} = \iint_S dS, \quad \mathbf{I_2} = \iint_S x_3 dS, \quad \mathbf{I_3} = \iint_S x_3^2 dS.$$

We introduce the notation for the right factor in the first term of the integrand of the second integral in Eq. (3.11):

$$\mathrm{EI}^* = \left(c - \frac{d^2}{a} \right) \mathbf{I_3} - \frac{2df}{a} \mathbf{I_2} - \left(\frac{f^2}{a} - g \right) \mathbf{I_1}. \tag{3.12}$$

The coefficient EI^* can be interpreted as the effective flexural rigidity of a flexoelectric beam.

We will assume that the electric field is linear in the thickness of the beam, then:

$$E_3 = -\frac{\partial \varphi}{\partial x_3} = \mathrm{const} = -\frac{v(t)}{h}, \tag{3.13}$$

where $v(t)$ is the electric potential between two electrodes on large surfaces of a beam, h is the thickness of a beam.

Since the measurement of the electrical voltage occurs at an electrical resistance R, the current flowing through the resistor will be equal to the time derivative of the averaged electric displacement D_3:

$$i(t) = \frac{v(t)}{R} = \frac{d}{dt} \left(\frac{1}{h} \iiint_V D_3 dV \right), \tag{3.14}$$

where $D_3 = -\varepsilon_0 \nabla \phi + P$. Taking into account Eq. (3.10), we obtain the equation of an electrical circuit with a flexoelectric coupling:

$$\frac{v(t)}{R} = -\frac{BL}{h} \left(\varepsilon_0 + \frac{1}{a} \right) \dot{v}(t) + \frac{1}{h} \int_0^L \left(\frac{d}{a} \mathbf{I_2} + \frac{f}{a} \mathbf{I_1} \right) \frac{\partial^2 \dot{w}}{\partial x_1^2} dx_1. \tag{3.15}$$

To solve the problem of forced vibrations of a flexoelectric beam, we will use the Kantorovich method [81]. We represent the relative displacements of a beam as a series expansion:

$$w(x_1,t)=\sum_{i=1}^{N}\eta_i(t)\phi_i(x_1), \tag{3.16}$$

where N is the number of vibration modes under consideration, $\eta_i(t)$ are unknown generalized coordinates, $\varphi_i(x_1)$ are known trial functions that satisfy the boundary conditions.

Substitute Eq. (3.13) and Eq. (3.16) in Eq. (3.11) and Eq. (3.15). In Eq. (3.11) we equate to zero the coefficients before the independent variation $\delta\eta$. We have obtained a system of two differential equations describing the forced oscillations of a flexoelectric beam, connected to a resistor:

$$\begin{aligned}&\mathbf{M}\ddot{\boldsymbol{\eta}}(t)+\mathbf{D}\dot{\boldsymbol{\eta}}(t)+\mathbf{K}\boldsymbol{\eta}(t)-\boldsymbol{\Theta}v(t)=\mathbf{p}\\&C_f\dot{v}(t)+\boldsymbol{\Theta}^{\mathrm{T}}\dot{\boldsymbol{\eta}}(t)+\frac{v(t)}{R}=0\end{aligned} \tag{3.17}$$

here:

$$\begin{aligned}C_f&=\frac{bL}{h}\left(\varepsilon_0+\frac{1}{a}\right),\\M_{ij}&=\int_0^L\rho\mathbf{I_1}\phi_i(x_1)\phi_j(x_1)dx_1,\\K_{ij}&=\int_0^L\mathrm{EI}^*\phi_i''(x_1)\phi_j''(x_1)dx_1,\\p_i&=\int_0^L\ddot{w}_c(t)\rho\mathbf{I_1}\phi_i\,dx_1,\\\Theta_i&=\int_0^L\frac{\phi_i''\,dx_1(x_1)}{h}\left(\frac{d}{a}\mathbf{I_2}+\frac{f}{a}\mathbf{I_1}\right)dx_1,\end{aligned} \tag{3.18}$$

where C_f is the effective capacity, b, h, and L are the width, height, and length of the piezoelectric element.

Now it remains to solve the problem of finding trial functions to satisfy the boundary conditions.

3.2.2 Boundary Conditions

To find $\varphi_i(x_1)$, we solve the problem of free vibrations for a beam clamped at both ends and having a proof mass at the center (see Fig. 3.1).

To take into account the influence of the proof mass M, located in the middle of the beam, we represent the function $\varphi_i(x_1)$ in the following form:

$$\phi_i(x_1) = \begin{cases} \phi_i^{(1)}(x_1), x_1 \leq \dfrac{L}{2} \\ \phi_i^{(2)}(x_1), x_1 > \dfrac{L}{2} \end{cases} \tag{3.19}$$

where $\phi_i^{(1)}(x_1)$ corresponds to the shape of the left half of the beam, and $\phi_i^{(2)}(x_1)$ corresponds to the right half.

In addition, it is necessary to take into account the influence of Min the system in Eq. (3.17). To do this, we add to Eq. (3.18) two components responsible for the influence of the mass M:

$$\begin{aligned} M_{ij} &= \int_0^L \rho \mathbf{I_1} \phi_i(x_1)\phi_j(x_1)dx_1 + M\phi_i\left(\frac{L}{2}\right)\phi_j\left(\frac{L}{2}\right), \\ p_i &= \int_0^L \ddot{w}_c(t)\rho \mathbf{I_1}\phi_i dx_1 + M\phi_i\left(\frac{L}{2}\right). \end{aligned} \tag{3.20}$$

We write the solution in common form for each part of the beam:

$$\begin{aligned} \phi_i^{(1)}(x_1) &= a_{1,i}\sin(\beta_i x_1) + a_{2,i}\cos(\beta_i x_1) + a_{3,i}\sinh(\beta_i x_1) + a_{4,i}\cosh(\beta_i x_1), \\ \phi_i^{(2)}(x_1) &= a_{5,i}\sin(\beta_i x_1) + a_{6,i}\cos(\beta_i x_1) + a_{7,i}\sinh(\beta_i x_1) + a_{8,i}\cosh(\beta_i x_1). \end{aligned} \tag{3.20}$$

We write out the boundary conditions for the ends of the beam and the coupling condition at the center of the beam:

$$\begin{aligned} &\phi_i^{(1)}\left(\frac{L}{2}\right) = \phi_i^{(2)}\left(\frac{L}{2}\right), \\ \phi_i^{(1)}(0) = 0, \quad &\phi_i^{(1)}\left(\frac{L}{2}\right) = \phi_i^{(2)\prime}\left(\frac{L}{2}\right), \quad \phi_i^{(2)}(L) = 0, \\ \phi_i^{(1)\prime}(0) = 0, \quad &\phi_i^{(1)\prime\prime}\left(\frac{L}{2}\right) = \phi_i^{(2)\prime\prime}\left(\frac{L}{2}\right), \quad \phi_i^{(2)\prime}(L) = 0, \\ &\phi_i^{(1)\prime\prime\prime}\left(\frac{L}{2}\right) = \phi_i^{(2)\prime\prime\prime}\left(\frac{L}{2}\right) - \alpha\beta^4\phi_i^{(1)}\left(\frac{L}{2}\right), \end{aligned} \tag{3.21}$$

where $\alpha = M/\rho \mathbf{I_1} L$

Satisfying the boundary conditions, we obtain a homogeneous system of eight equations with eight unknowns:

$$\Lambda = \begin{pmatrix} a_{1,1} & \cdots & a_{1,8} \\ \vdots & \ddots & \vdots \\ a_{8,1} & \cdots & a_{8,8} \end{pmatrix} \tag{3.22}$$

We need to find the determinant of this system in order to find the eigenvaluesβ_i. Since $\det(\Lambda) = 0$ is a transcendental equation, we will search for its solution using numerical methods. Having obtained the set of β_i, we calculate the coefficients a_i for the required number of modes of oscillations N.

3.2.3 Solution

Since we will consider the case of harmonic excitation of the base, the stages of finding the solution will be similar to those given in Chap. 1 for cantilever-type PEGs. The solution for the system of equations (Eq. 3.17) has the form:

$$\begin{aligned}\widetilde{\boldsymbol{\eta}} &= \left[-\omega^2\mathbf{M} + i\omega(\mu\mathbf{M} + \gamma\mathbf{K}) + \mathbf{K} + \frac{i\omega\boldsymbol{\Theta}\boldsymbol{\Theta}^T}{i\omega C_f + \frac{1}{R}}\right]^{-1}\tilde{\mathbf{p}} \\ \tilde{v} &= -\frac{i\omega\boldsymbol{\Theta}^T}{i\omega C_f + \frac{1}{R}}\left[-\omega^2\mathbf{M} + i\omega(\mu\mathbf{M} + \gamma\mathbf{K}) + \mathbf{K} + \frac{i\omega\boldsymbol{\Theta}\boldsymbol{\Theta}^T}{i\omega C_f + \frac{1}{R}}\right]^{-1}\tilde{\mathbf{p}}\end{aligned} \tag{3.23}$$

3.2.4 Numerical Experiment

As input parameters of the model, we use the initial data from the experiment. We will consider a piezoceramic beam made of unpolarized ceramic PZT-19, which has the geometric and physical properties given in Table 3.1 [24, 94, 98].

Since unpolarized ceramics is a material with central symmetry, the piezoelectric modulus d of such a material will be equal to zero. The inverse dielectric susceptibility was calculated using the formula $a = (\varepsilon\varepsilon_0 - \varepsilon_0)^{-1}$, and the flexoelectric module is $f = -a\mu_{12}$. The amplitude of the displacement of the base is $\tilde{w}_c = 0.03$ mm. The coefficients of the modal damping are $\xi_1 = \xi_2 = 0.02$.

Let us construct the amplitude-frequency characteristics of the motion of the middle of the beam and the electric voltage for various load resistances. The calculated resonance frequency is 504 Hz.

Figure 3.4 shows that the maximum displacement at resonance is 1 mm.

The values of the electrical voltage, shown in Fig. 3.5, differ from those obtained in the experiment described in the beginning of this chapter.

Since the definition of material constants affecting higher-order effects (such as the flexoelectric effect) is a complex and not completely solved research problem, in our case we can try to vary the coefficient μ_{12}.

During the variation of the coefficient, it was found that when a certain value of the coefficient is reached, the effective flexural rigidity EI^* becomes negative.

Table 3.1 Parameters of the ferroelectric ceramic beam

	Piezoelement
Geometrical dimensions ($L_0 \times b \times h$)	$50 \times 4 \times 0.7$ mm^3
Length of working part of the specimen (L)	35 mm
Density (ρ)	7,280 kg/m^3
Elastic modulus (c)	114.8 GPa
Elastic compliance $\left(s_{11}^E\right)$	17.5×10^{-12} Pa
Relative permittivity $\left(\varepsilon_{33}^S/\varepsilon_0\right)$	682.6
Inverse dielectric susceptibility (a)	0.166 GNm^2/C^2
Flexoelectrical factor (μ_{12})	2 μC/m
Flexoelectrical modulus (f)	−331 Nm/C
Higher order elastic modulus (g)	1.75 μN

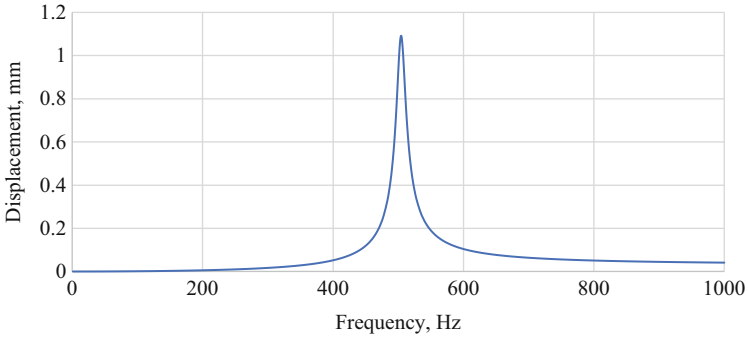

Fig. 3.4 Frequency response of the beam's center displacement, obtained from the numerical experiment

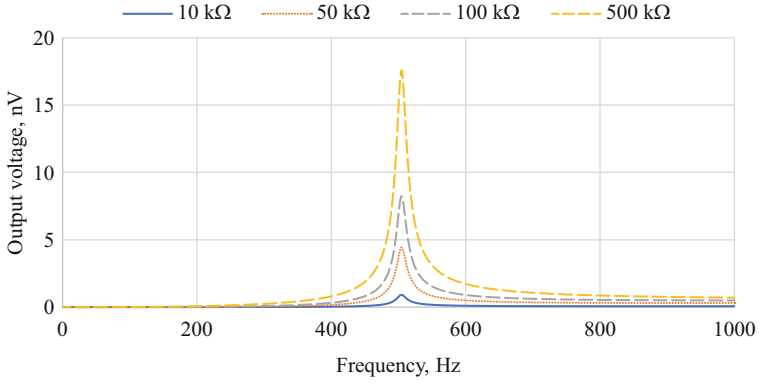

Fig. 3.5 Frequency response of output voltage across the resistor with different values of the load resistance, obtained from the numerical experiment

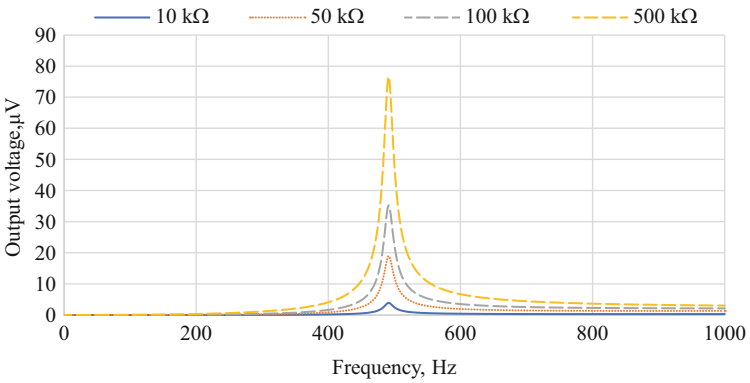

Fig. 3.6 Frequency response of the voltage across the resistor with different values of the load resistance, obtained from the numerical experiment

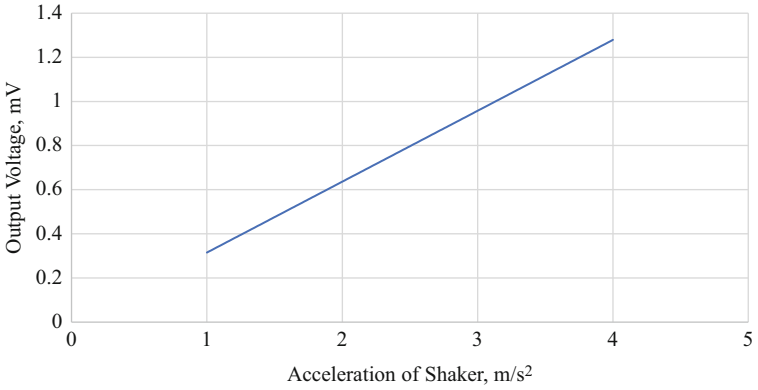

Fig. 3.7 Dependence of the electrical response on the acceleration of the shaker, measured at the resonance frequency at R= 360 kΩ and M = 3.1 g

Therefore, we chose the nearest value in the vicinity of the transition point, equal to 10^{-3}, and built the amplitude-frequency characteristic of the electric voltage.

Figure 3.6 shows that the values of the electrical voltage increased by three orders of magnitude. Nevertheless, these values are sufficiently small in comparison with the experimental values. In addition, the resonance frequency slightly decreased to 491 Hz. The amplitude of the displacement of the middle of the beam remained unchanged. Such a difference may indicate inaccurate input data, as well as the nonlinearity of the phenomenon under study.

At the beginning of the chapter in Fig. 3.2, the dependencies of the output electric voltage on the table acceleration are presented. Let us construct an analogous dependence.

The values of the output voltage presented in Fig. 3.7 are quantitatively different from the experimental values, nevertheless, they qualitatively reflect the dependence

of the electric voltage on acceleration. Such a difference may indicate inaccurate input data, as well as the nonlinearity of the phenomenon under study.

The results obtained in the course of the numerical experiment showed the possibility of the appearance of an electric potential in an unpolarized piezoceramic beam and its qualitative characteristics.

3.3 Conclusion

The main result of this chapter is the formulation of the problem of forced oscillations of an unpolarized ferroelectric beam in the presence of proof mass, taking into account the flexoelectric effect.

It is shown that the output electric potential can arise in unpolarized samples, and its values can serve to determine the flexoelectric constants.

It is found that the variation of such a constant is possible only up to a certain point, when the effective stiffness EI becomes negative, and the results lose physical meaning.